Chemical Physics Letters 468 (2009) 264–269

Contents lists available at ScienceDirect

Chemical Physics Letters

journal homepage: www.elsevier.com/locate/cplett

Strong-field ionization of sputtered molecules for biomolecular imaging

D. Willingham, A. Kucher, N. Winograd *

Chemistry Department, Pennsylvania State University, 104 Chemistry Building, University Park, PA 16802, USA

ARTICLE INFO

Article history:
Received 29 September 2008
In final form 18 November 2008
Available online 7 December 2008

ABSTRACT

Photoionization of molecules sputtered from molecular thin films has been achieved using high field 125 fs pulses in the mid-IR spectral range. Using several model systems, we show that it is possible to significantly reduce molecular fragmentation induced by the laser field by increasing the photoionization wavelength. By examining the photoionization spectra as a function of wavelength, it is apparent that the photoionization mechanism is changing from a non-adiabatic multi-electron excitation process to a process that involves tunnel ionization. The results of these observations are discussed in terms of their significance for bioimaging with focused ion beams and mass-spectrometry.

1. Introduction

Lasers have been utilized to create ions for mass-spectrometry-based experiments, almost since their invention. For the last 25 years, a number of groups have been particularly interested in using laser-based photoionization to detect neutral atoms and molecules desorbed from surfaces, either by energetic ion beams or by photons [1–6]. Usually, secondary ions produced during the desorption process, either by electronic excitation or by direct collisions, are detected directly by the time-of-flight mass-spectrometry (TOF-MS). The number of these ions is generally quite small, less than one in 100 000, and may not be representative of how the ensemble of desorbed material is behaving. Hence, laser-based photoionization of the neutral component can provide important fundamental information, and offers the opportunity of increasing the sensitivity of these types of measurements. This enhanced sensitivity is crucial in order to perform molecule-specific bioimaging experiments using focused ion beams [7,8].

An array of technologies has been brought to bear on this problem, ranging from single-photon ionization using lasers [9] or synchrotron radiation [10,11] to resonant [1,2,5,12] and non-resonant multiphoton ionization [3,13–17]. Early studies using ion beams to desorb atomic species proved successful since atoms can be resonantly photoionized with nearly 100% efficiency using many different schemes [5]. This strategy, although not widely employed, has been successful for detecting trace elements in semiconductors and in determining isotope ratios in extraterrestrial dust grains [18]. Experiments involving the photoionization of molecules have been much less successful, however, due to the fact that the laser field inevitably produces photofragmentation products that reduce the overall ionization efficiency and increase congestion in the photoionization mass spectrum [16]. More recent experiments utilizing high field femtosecond pulsed Ti:sapphire lasers have been modestly successful in yielding simplified spectra with good ionization efficiency, but effects of the high field and the presence of a broad distribution of internal energies associated with desorbed molecules have conspired to reduce the broad appeal of this technology [19].

Although some authors have observed reduced molecular fragmentation by decreasing the photoionizing wavelength [13], recent experiments suggest that softer photoionization is possible by employing high field fs pulses at longer wavelengths [20–26]. The basis for this idea is that when strong-field, long wavelength laser beams interact with atoms and small molecules, the ionization mechanism enters a regime whereby the most weakly bound electron tunnels through a quasi-static barrier formed by the superposition of the core potential with the laser electric field. For example, decatetraene exhibits a transition from nearly fragment-free photoionization using 40 fs pulses of 1450 nm radiation at 10^{14} W/cm^2 to complete fragmentation at 800 nm using 10^{13} W/cm^2 [21]. Although the saturation thresholds for polyatomic molecules are typically higher at longer wavelengths, the reduction in photodissociation is the dominant factor leading to substantial increases in the ionization efficiencies for polyatomic molecular ion species.

The nature of the barrier suppression may be viewed as static when the tunneling occurs on a timescale much less than that of the laser period. Although this view of strong-field ionization rests heavily on the quasi-static and single active electron (SAE) approximations, it has been successfully applied in the past. The Keldysh parameter (γ), derived from the classical view of tunnel ionization, suggests that the wavelength dependence upon the tunneling probability is small compared to the dependence on the laser intensity; however, recent reports indicate that polyatomic molecular systems exhibit a stronger wavelength dependence than

* Corresponding author. Fax: +1 814 863 0618.
E-mail address: dgw140@psu.edu (N. Winograd).

0009-2614/$ - see front matter © 2008 Elsevier B.V. All rights reserved.
doi:10.1016/j.cplett.2008.11.094

was previously thought [20–23]. For these systems, the quasi-static and SAE approximations are believed to breakdown and ionization is controlled by either an adiabatic or a non-adiabatic multi-electron (NME) process where the wavelength dependence of the photoionization rate may be much different than the classical prediction [24–26].

In this Letter, we report preliminary experiments using high field fs mid-IR laser pulses to detect different types of molecules desorbed from surfaces by energetic ion bombardment. The goal is to capitalize on the reduced photofragmentation observed in this regime and to determine if this approach can lead to a more general strategy for increasing the ionization efficiency in mass-spectrometry experiments. We specifically focus on the photoionization mass spectra obtained between 800 nm and 2000 nm to determine the optimum conditions for minimizing photofragmentation and to determine if there are detrimental effects of the broad internal energy distribution associated with these sputtered molecules. The results show that for the polyaromatic hydrocarbon molecule coronene and for the heterocyclic aromatic compounds guanine and histamine that the fragmentation is greatly reduced at wavelengths of 1450 nm and above, although significant differences in the mass spectra are still observed between sputtered molecules and thermally evaporated molecules. Due to this decrease in photofragmentation, there is adequate sensitivity for molecular ions to perform chemical imaging experiments using focused ion beams. The results are discussed in terms of a non-resonant adiabatic excitation model for molecular tunnel ionization.

2. Experimental

Experiments were performed using a TOF-MS instrument which has been described in detail, previously [15]. Molecules were desorbed using a pulsed 40 keV C_{60} ion source (Ionoptika, Ltd.) by focusing a 50 pA beam, measured in direct current mode, to a 5 μm diameter spot on the sample. To ensure that a broad velocity distribution of desorbed molecules is sampled by the laser, this pulse width was set to 2 μs. The photoionization source then interacts with the sputtered molecules through a calcium fluoride (CaF_2) window that is transparent to all wavelengths used in this study. The ionization volume is confined to a cylindrical area approximately 500 μm above the surface, 250 μm in diameter, and 1 mm in length. Once the molecules are ionized, they are then extracted with 2550 V into a reflectron-type TOF apparatus and detected at a multichannel plate ion detector. Secondary ions formed directly by collisions with the incident projectile are mass selected by a delayed 2500 V pulse which extracts ions into the TOF. These ions are then detected using a multichannel plate detector. The data acquisition is performed by a PDA500 transient digitizer.

The ionization source is an optical parametric amplifier (OPA) pumped by a femtosecond laser. The pump system consists of a self-mode-locked Ti:sapphire oscillator (Clark-MXR, Inc.) pumped by the 4 W output of a Verdi V5 diode-pumped laser (Coherent, Inc.). The 800 nm, 100 MHz, 3 nJ, 100 fs output of the oscillator is sent to a single grating, multipass stretcher where the beam is stretched to ~300 ps and then amplified by a Ti:sapphire regenerative amplifier. The 800 nm, 1 kHz, 1.5 mJ, 300 ps output from the regenerative amplifier is further amplified by a second stage multipass amplifier and then compressed using a multipass single grating compressor. The final pump output is characterized by 800 nm, 1 kHz, 1.5 mJ, 125 fs. The mid-IR source of radiation is generated by a traveling-wave OPA of white light continuum (TOPAS) developed by Light Conversion Ltd. and distributed by Coherent Inc. The TOPAS operates by splitting the energy of a pump photon into two photons whose summed energy is that of the total energy of the pump photon. The energy difference between the two photons, and therefore their wavelengths, may be tuned. The combined signal and idler output from the TOPAS pumped by the femtosecond system is characterized by 1 kHz, 400 μJ, 125 fs laser pulses. The wavelength output may be tuned from 1150–2650 nm. The output power of the TOPAS system was controlled manually by rotating a half-wave plate within the compressor of the femtosecond pump system resulting in half-wave plate-polarizer attenuation. Although spectral modulation, decreased pulse width and change of pulse shape are likely to occur when attenuating femtosecond laser pulses, a recent study has shown that these effects are much less prominent with half-wave plate-polarizer attenuators than with alternative absorption or reflection type attenuation techniques [27]. The power density ranges between 10^{12} and 10^{13} W/cm^2 after focusing the beam to the chamber center using a 125 mm lens.

Guanine (>98.0%, CAS 73-40-5), coronene (>97.0%, CAS 191-07-1), and histamine (>97.0%, CAS 51-45-6) were purchased from Sigma–Aldrich and used without any further purification. All samples were prepared by physical vapor deposition (PVD) in vacuo onto precut 5 × 5 × 0.5 mm silicon wafers (Product No: 16008) purchased from Ted Pella, Inc. The first step of the PVD process involves the heating of an aluminum oxide crucible containing the target molecules with a tungsten filament to reach vaporization. Next, the gas-phase molecules pass through a diffusion grid to achieve an equilibrium composition across the entire deposition area. Finally, the gas-phase molecules are condensed onto silicon wafers cooled by liquid nitrogen forming a pure, uniform molecular film. The surface roughness of such films has been measured by atomic force microscopy at about 5 nm route mean squared [28]. The thickness of the molecular films may be monitored by a quartz crystal microbalance and may range from several angstroms to several micrometers. All films used in this study were between 200 and 300 nm thick.

3. Results and discussion

The aim of this work is to experimentally examine the influence of laser wavelength on the high field fs photoionization mass spectra of polyatomic sputtered molecules. The theoretical guidance for these experiments is complicated by the interaction of the intense laser pulse with the electronic system of the molecule. A quasi-static single active electron (SAE) approximation has been successfully applied to simple systems whereby barrier suppression rather than high order photon absorption is the dominant mechanism. These two processes may be distinguished using the Keldysh parameter, γ, traditionally used to evaluate the behavior of atoms in strong laser fields as

$$\gamma = \left[\frac{IP}{(1.87 \times 10^{-13} I\lambda^2)}\right]^{1/2}$$

where IP is the ionization potential, I is the laser power density in W/cm^2, and λ is the wavelength in μm. It is thought that multiphoton absorption dominates when $\gamma > 5$ and barrier suppression ionization prevails when $\gamma < 0.5$ [17]. At values between these two numbers, the ionization occurs by two competing and indistinguishable ionization mechanisms. To achieve $\gamma \ll 5$, it is necessary to increase either the laser power density and/or the laser wavelength. It is unclear, however, whether the Keldysh parameter accurately describes the behavior of molecular species within a strong laser field. The values of γ utilized in this work range from 1.20 at 1450 nm to 2.17 at 800 nm at a laser power of 400 mW.

A second approach involves non-adiabatic multi-electron (NME) processes where coupling of electronic states can lead to multiphoton absorption, usually followed by photofragmentation.

The half-cycle transition probability of NME has been estimated from the Landau–Dykhne formalism as

$$P \sim \exp(-\pi \Delta_0^2 / 4\omega_L \varepsilon \mu)$$

where Δ_0 is the energy separation between the ground state and the onset of the quasi-continuum coupled with dipole matrix element μ. The electric field, ε, oscillates with frequency ω_L. Hence, to avoid non-adiabatic excitations, $4\omega_L \varepsilon \mu \ll \pi \Delta_0^2$ For complex polyatomic molecules, it is not clear whether either of these two formalisms can accurately predict the wavelength dependence of the photoionization mass spectra, but both approaches suggest that longer wavelengths will more readily allow tunnel ionization while reducing the effects of multiphoton absorption.

Typical photoionization spectra for two different molecules sputtered directly from a thin film using a 40 keV incident C_{60} probe are shown in Fig. 1. The first example is coronene, an aromatic hydrocarbon with molecular weight 300.2 Dalton. Earlier high field photoionization experiments with these types of molecules showed that for extended π systems, the probability of NME is large resulting in more fragmentation. As seen in Fig. 1a, photoionization at 800 nm yields a spectrum with little evidence for a molecular ion, along with a series of fragment ions assigned to carbon clusters containing from 1 to 13 carbon atoms. When the wavelength is increased to 1450 nm, however, the molecular ion at m/z 300.2 appears with considerable intensity. Moreover, the molecular weight distribution of the carbon cluster fragment ions is shifted to a slightly higher value. This effect may be seen quantitatively by evaluating the percentage of fragment peaks in the mass range of 0–50 amu compared to those in the range of 51–200 amu for both the 800 nm and 1450 nm photoionization mass spectra. Close evaluation of the mass spectra in these mass ranges shows that approximately 6% of the fragment peaks have shifted from the 0–50 amu mass range to the 51–200 amu mass range when comparing the 1450 nm mass spectrum to the 800 nm mass spectrum. A more dramatic effect is observed for the heterocyclic aromatic nucleotide, guanine, as shown in Fig. 1c and d. Photoionization of sputtered guanine at 800 nm yields only small fragment ions at m/z 43 and 27, presumably associated with the $CH_3N_2^+$ and CHN^+, respectively. Photoionization at 1450 nm yields mainly the molecular ion at m/z 151.13. Clearly, in both of these cases, even though the molecules possess a range of internal energies imparted by the sputtering process, the photoionization mechanism is changing as the wavelength is increased.

Strong-field photoionization has the potential to increase sensitivity for molecular species desorbed by an energetic C_{60} ion beam. A comparison between the secondary ion mass spectrum (SIMS) and the 1450 nm photoionization mass spectrum of coronene molecules desorbed from a thin film by 40 keV C_{60} primary ions is shown in Fig. 2. Although the photoionization spectrum shows more fragment ions, there is an order of magnitude increase in the sensitivity for molecular ions over the SIMS ions due to a substantial increase in the overall signal of all ions. For all molecules studied to date, the 1450 nm photoionization molecular ion signals are on the order of or are greater than those observed for the SIMS ions. To examine the influence of the sputtering process on the wavelength dependence of the photoionization process, we next compare the photoionization spectra of histamine, an aromatic amino acid, when it is produced by thermal evaporation and when it is produced by sputtering. This system has been extensively studied previously at 800 nm, where the photoionization mechanism was established to involve non-resonant multiphoton excitation. As shown in Fig. 3a, photoionization channels originate from the α-cleavage of the carbon–carbon bond in the alkyl chain portion of the histamine molecule [16]. The first fragment ion channel is indicative of the aminomethyl cation $CH_2NH_2^+$ at m/z 30, while the second channel is a product of the corresponding $[M–CH_2NH_2]^+$ at m/z 81. The major fragment at m/z 82 arises from a radical site McLafferty rearrangement and is enhanced by the presence of an aromatic moiety adjacent to the ethylamine portion of the molecule, which acts to stabilize the charge deficiency through delocalization of the ring electrons. The molecular ion at m/z 111.15 is easily observable. When the wavelength is increased to 1450 nm, the spectrum is similar to the 800 nm spectrum, except that the m/z 30 and m/z 81 fragments are not formed, and the intensity of the molecular ion is increased relative to that observed at m/z 82.

During the sputtering process, as noted above, the molecules pick up a distribution of internal energies, and fragmentation may occur during the desorption process. It is not generally possible for us to distinguish between this scenario and fragmentation caused by the laser field. Typically, the molecular ion of histamine

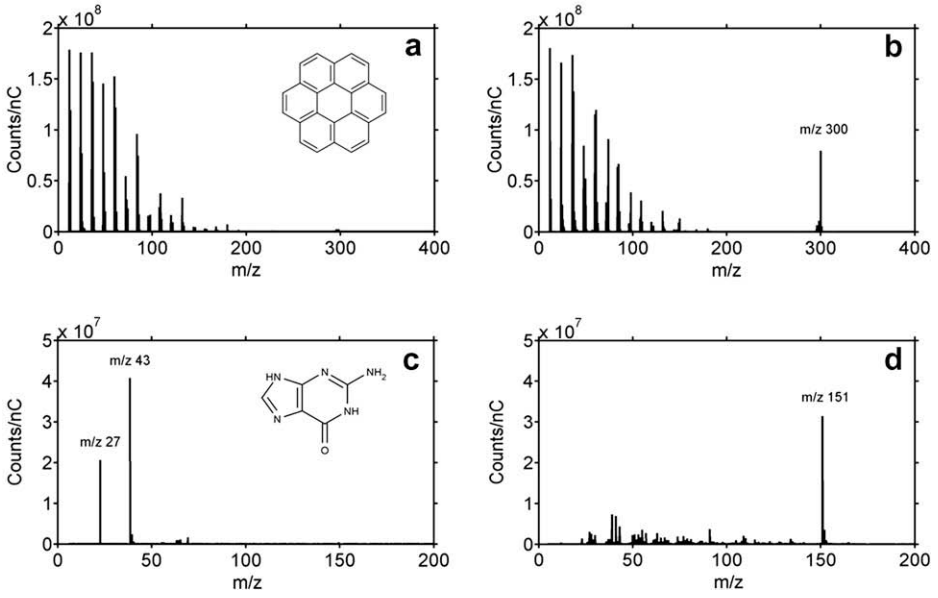

Fig. 1. Wavelength dependence of photoionization mass spectra of coronene (a,b) and guanine (c,d) produced by bombardment of a thin film with 40 keV C_{60} primary ions. The photoionization mass spectra (a,c) were obtained using 800 nm and (b,d) using 1450 nm laser pulses. The y-axis (counts/nC) in (a,b,c,d) is related to the number of ions obtained per C_{60} primary ion.

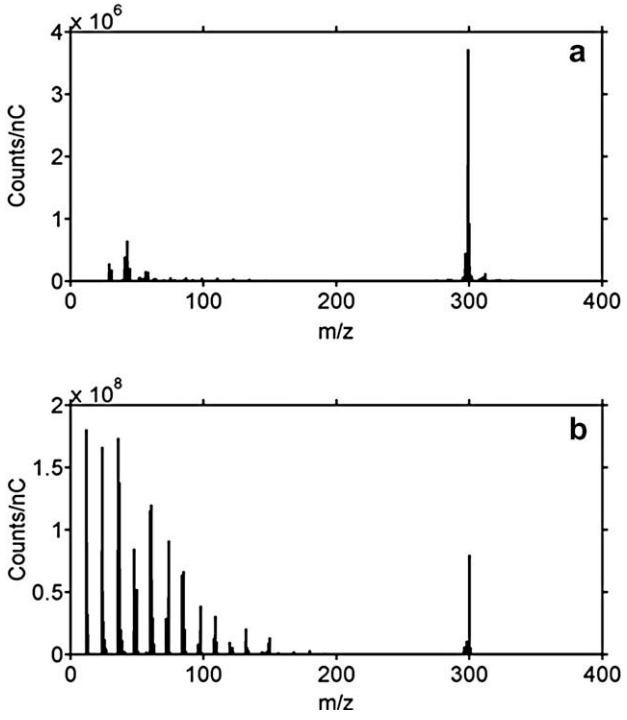

Fig. 2. Comparison of the secondary ion mass spectra (a) and the 1450 nm photoionization mass spectra (b) of a coronene thin film produced by bombardment with 40 keV C_{60} primary ions using 1 kHz, 400 mW, 125 fs laser pulses for ionization. The y-axis (counts/nC) is related to the number of ions detected per incident C_{60} ion.

at *m*/*z* 111.15 is not observed after photoionization with fs pulses using wavelengths between 200 nm and 800 nm [29]. However, as the wavelength is increased, as illustrated in Fig. 2c and d, the molecular ion emerges, and the low mass fragmentation pattern shifts dramatically to higher masses. These data provide additional evidence for a change in the photoionization mechanism.

It can be concluded from the data shown here that strong-field effects are, indeed more prevalent at longer wavelengths, whereas high order photon absorption processes tend to dominate at shorter wavelengths. This observation may be examined in more detail by comparing the mass-to-fragment ratio (M^+/F_{tot}), defined as the total integrated counts of the molecular ion species (M^+) divided by the total integrated counts of all masses less than that of the molecular ion species (F_{tot}), over the available wavelength tuning range. Wavelength tuning is achieved through a software controlled optical delay line and the rotation of the non-linear BBO crystal within the TOPAS system. The M^+/F_{tot} response for histamine sputtered neutral molecules as a function of wavelength in the range of 1200–2000 nm is shown in Fig. 4a. Individual wavelengths were separated using a broadband tunable laser mirror that reflects the signal wavelength and transmits the idler wavelength. The wavelengths shown in Fig. 4a are single wavelengths only. Note that a significant suppression of fragment ions begins to occur at just above 1800 nm.

The M^+/F_{tot} ratio may be applied to the molecular ion response of histamine molecules as a function of laser power density. In this case, gas-phase histamine molecules were used instead of the sputtered molecules in order to obtain a greater sensitivity for photoionized molecular ions. Power densities were attenuated by adjusting the rotation of a half-waveplate positioned inside the pulse compressor of the femtosecond pump system prior to pulse compression. With this configuration the compression grating acts as a polarizer due to the fact that the grating reflectivity is sensitive to the polarization of the incoming laser beam [27]. We believe that this is the most effective way to attenuate the output of the TOPAS without largely affecting other beam parameters.

The power dependence data presented in Fig. 4b contains unexpected experimental results. As the power density increases, the M^+/F_{tot} ratio increases as shown in Fig. 4b, but eventually the M^+/F_{tot} ratio saturates with increasing power density. The initial increase in the M^+/F_{tot} ratio can easily be explained by an increase in ionization efficiency at higher power densities; although, one would expect the signal to reach a threshold point where photodissociation pathways begin to dominate. The typical response resulting from this behavior is a quick drop in the M^+/F_{tot} ratio indicating

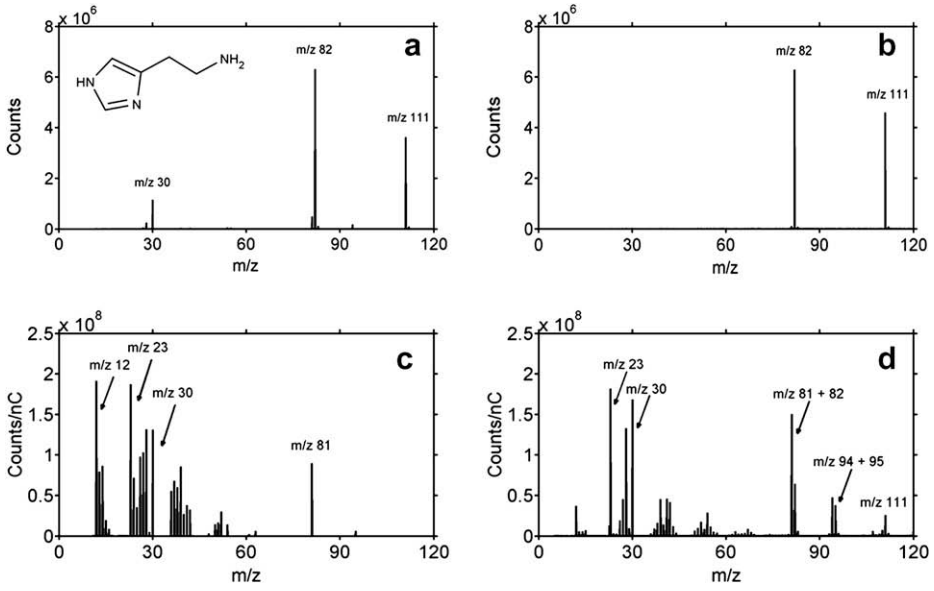

Fig. 3. Wavelength dependence of the photoionization mass spectra of thermally evaporated histamine (a,b) and histamine desorbed by 40 keV C_{60} primary ions (c,d) using 1 kHz, 400 mW, 125 fs laser pulses for ionization. The photoionizing wavelengths used are 800 nm (a,c) and 1450 nm (b,d). To obtain the thermal data, a thin film of histamine was heated to 50 °C, a temperature adequate to release sufficient number of molecules into the gas-phase for detection. The y-axis (counts) in (a,b) is the direct signal obtained; however, the y-axis (counts/nC) in (c,d) is dependent on the C_{60} primary ion current.

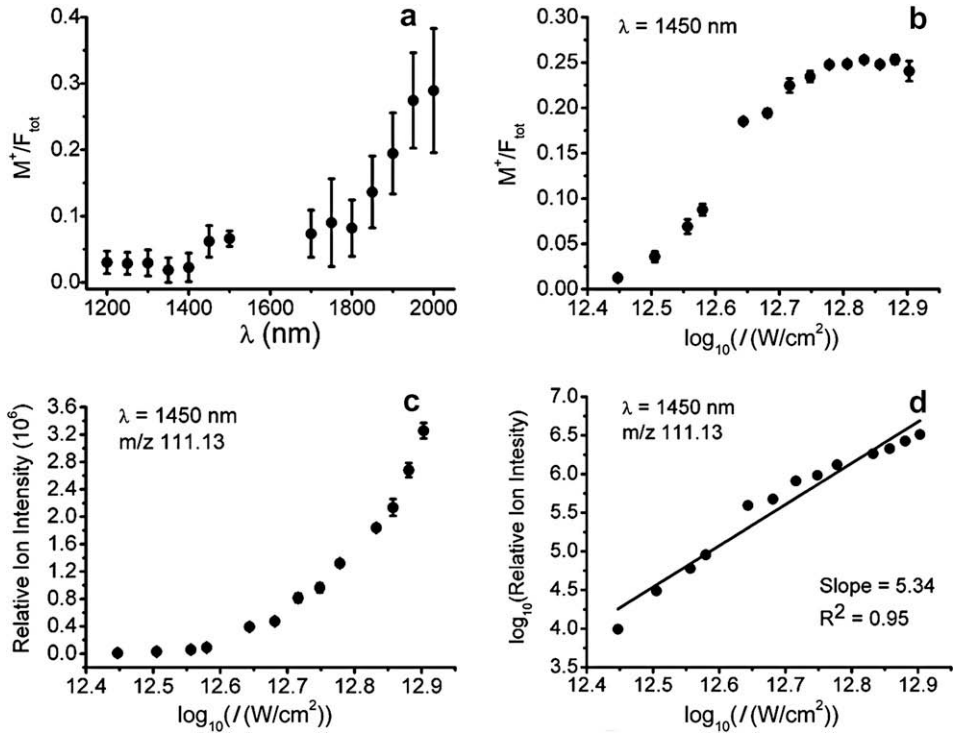

Fig. 4. Wavelength and power dependence of photoionization spectra for thermally evaporated histamine molecules. The wavelength dependence of the M^+/F_{tot} ratio is shown in (a) using 4×10^{12} W/cm^2 of laser power density at each wavelength. The power dependence of the M^+/F_{tot} ratio is shown in (b) using a fixed wavelength of 1450 nm. The change in molecular ion signal with laser power density at m/z 111.13 is shown in (c). The change in the log of the molecular ion signal with laser power density at m/z 111.13 is shown in (d) and the slope and R^2 values are reported.

extensive amounts of photofragmentation as a result of imparting excess internal energy into the molecules of interest. As can be seen in Fig. 4b, the M^+/F_{tot} ratio does increase at first, but does not decrease with increased power density as expected. Fig. 4c shows that although the M^+/F_{tot} ratio remains constant past a given value, the intensity of M^+ at m/z 111.13 continues to increase exponentially. Concerns of ionization volume changes may be raised when comparing various wavelengths and power densities; however, when signal ratios are used changes in the ionization volume are not important since all signals should be proportional to the ionization volume. Furthermore, the log–log plot shown in Fig. 4d exhibits a slope of 5.34. Increases in the ionization volume typically result in a slope of approximately 1.5 for these types of plots. It is clear that expansion of the ionization volume represents a portion of the slope; however, there is a significant contribution of increased ionization at higher power densities to this number. Once again, these observations indicate that the ionization mechanism present at longer wavelengths and higher power densities is more characteristic of strong-field tunnel ionization rather than NME.

These preliminary results greatly improve the prospect for utilizing this strategy for bioimaging experiments. Imaging is achieved by focusing the 40 keV C_{60} primary ion beam to a spot size of about 1 μm. The focused beam is then rastered across the sample acquiring mass spectra at each pixel position. The mass spectral information may then be used to generate a 256×256 pixel chemical specific image. The image shown in Fig. 5 is that of a patterned vapor-deposited thin film of the purine adenine on a silicon substrate.

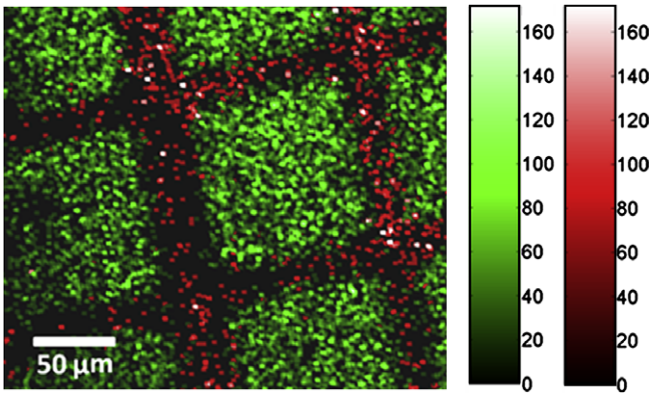

Fig. 5. Image of a patterned PVD thin film of adenine on a silicon substrate acquired using a 40 keV focused C60 probe. The image consists of 256×256 individual mass spectra. The adenine molecular ion m/z 135.13 is indicated in green and the silicon substrate m/z 28.09 is indicated in red.

4. Conclusion

In this Letter, we report the photoionization spectra for several biomolecules desorbed from molecular thin films by a focused cluster ion beam. Utilizing strong-field photoionization in the mid-IR spectral region has led to a substantial reduction in the amount of photofragmentation typically observed at shorter wavelengths. This reduction in photofragmentation provides adequate sensitivity for chemical imaging of organic and biological samples.

The results presented here are of a preliminary nature, but are sufficient to suggest that this approach may considerably expand the utility of lasers as molecular ionization tools. The present data, along with advancements in the theory, suggest that experiments performed at even longer wavelengths and higher power using polarized light may further improve the quality of the spectra.

Acknowledgements

Financial support from the National Institute of Health under Grant # EB002016-15, and the Department of Energy Grant # DE-FG02-06ER15803 are acknowledged. We also thank Robert Levis and Andreas Wucher for their many consultations.

References

[1] S.D. Kramer et al., Radiocarbon 22 (1980) 428.
[2] N. Winograd, J.P. Baxter, F.M. Kimock, Chem. Phys. Lett. 88 (1982) 581.
[3] C.H. Becker, K.T. Gillen, Analytical Chemistry 56 (1984) 1671.
[4] M.J. Pellin, C.E. Young, W.F. Calaway, D.M. Gruen, Surf. Sci. 144 (1984) 619.
[5] D.L. Pappas, D.M. Hrubowchak, M.H. Ervin, N. Winograd, Science 243 (1989) 64.
[6] D.S. McKay et al., Science 273 (1996) 924.
[7] N. Winograd, Anal. Chem. 65 (1993) A29.
[8] M. Wood, Y. Zhou, C.L. Brummel, N. Winograd, Anal. Chem. 66 (1994) 2425.
[9] U. Schuhle, J.B. Pallix, C.H. Becker, J. Am. Chem. Soc. 110 (1988) 2323.
[10] E.R. Mysak, K.R. Wilson, M. Jimenez-Cruz, M. Ahmed, T. Baer, Anal. Chem. 77 (2005) 5953.
[11] K.R. Wilson, L. Belau, C. Nicolas, M. Jimenez-Cruz, S.R. Leone, M. Ahmed, Int. J. Mass Spectrom. 249 (2006) 155.
[12] D.M. Hrubowchak, M.H. Ervin, M.C. Wood, N. Winograd, Anal. Chem. 63 (1991) 1947.
[13] C.L. Brummel, K.F. Willey, J.C. Vickerman, N. Winograd, Int. J. Mass Spectrom. Ion Process. 143 (1995) 257.
[14] K.F. Willey, C.L. Brummel, N. Winograd, Chem. Phys. Lett. 267 (1997) 359.
[15] K.F. Willey, V. Vorsa, R.M. Braun, N. Winograd, Rapid Commun. Mass Spectrom. 12 (1998) 1253.
[16] V. Vorsa, T. Kono, K.F. Willey, N. Winograd, J. Phys. Chem. B 103 (1999) 7889.
[17] V. Vorsa, K.F. Willey, N. Winograd, Anal. Chem. 71 (1999) 574.
[18] K. McKeegan et al., Meteoritics Planet. Sci. 41 (2006) A19.
[19] D. Willingham, A. Kucher, N. Winograd, Molecular depth profiling and imaging using cluster ion beams with femtosecond laser postionization, Appl. Surf. Sci. 255 (2008) 831.
[20] M. Lezius, V. Blanchet, D.M. Rayner, D.M. Villeneuve, A. Stolow, M.Y. Ivanov, Phys. Rev. Lett. 86 (2001) 51.
[21] M. Lezius, V. Blanchet, M.Y. Ivanov, A. Stolow, J. Chem. Phys. 117 (2002) 1575.
[22] A.N. Markevitch, S.M. Smith, D.A. Romanov, H.B. Schlegel, M.Y. Ivanov, R.J. Levis, Phys. Rev. A 68 (2003).
[23] A.N. Markevitch, D.A. Romanov, S.M. Smith, H.B. Schlegel, M.Y. Ivanov, R.J. Levis, Phys. Rev. A 69 (2004).
[24] S.M. Smith, X.S. Li, A.N. Markevitch, D.A. Romanov, R.J. Levis, H.B. Schlegel, J. Phys. Chem. A 109 (2005) 10527.
[25] S.M. Smith, X.S. Li, A.N. Markevitch, D.A. Romanov, R.J. Levis, H.B. Schlegel, J. Phys. Chem. A 109 (2005) 5176.
[26] S.M. Smith, X.S. Li, A. Markevitch, D. Romanov, R.J. Levis, H.B. Schlegel, J. Phys. Chem. A 111 (2007) 6920.
[27] Y.B. Zhao, Y.Q. Jia, J.J. Yang, X.N. Zhu, Opt. Eng. 46 (2007).
[28] J. Kozole, A. Wucher, M. Winograd, Anal. Chem. 80 (2008) 5293.
[29] A. Wucher, S.X. Sun, C. Szakal, N. Winograd, Anal. Chem. 76 (2004) 7234.